Journal of
Plankton Research

plankt.oxfordjournals.org

J. Plankton Res. (2016) 38(2): 230–243. First published online December 17, 2015 doi:10.1093/plankt/fbv107

Costa Rica Dome: Flux and Zinc Experiments

Biomass and composition of protistan grazers and heterotrophic bacteria in the Costa Rica Dome during summer 2010

ALEXANDRA FREIBOTT[1]*, ANDREW G. TAYLOR[1], KAREN E. SELPH[2], HONGBIN LIU[3], WUCHANG ZHANG[4] AND MICHAEL R. LANDRY[1]

[1]SCRIPPS INSTITUTION OF OCEANOGRAPHY, UNIVERSITY OF CALIFORNIA AT SAN DIEGO, 9500 GILMAN DR., LA JOLLA, CA, USA, [2]DEPARTMENT OF OCEANOGRAPHY, UNIVERSITY OF HAWAII AT MANOA, HONOLULU, HI, USA, [3]THE HONG KONG UNIVERSITY OF SCIENCE AND TECHNOLOGY, HONG KONG SAR, CHINA AND [4]INSTITUTE OF OCEANOGRAPHY, CHINESE ACADEMY OF SCIENCE, QINGDAO, CHINA

*CORRESPONDING AUTHOR: afreibott@ucsd.edu

Received May 11, 2015; accepted November 19, 2015

Corresponding editor: John Dolan

We investigated biomass and composition of heterotrophic microbes in the Costa Rica Dome during June–July 2010 as part of a broader study of plankton trophic dynamics. Because picophytoplankton (<2 μm) are known to dominate in this unique upwelling region, we hypothesized tight biomass relationships between size-determined predator–prey pairs (i.e. picoplankton–nano-grazers, nanoplankton–micro-grazers) within the microbial community. Integrated biomass of heterotrophic bacteria ranged from 180 to 487 mg C m^{-2} and was significantly correlated with total autotrophic carbon. Heterotrophic protist (H-protist) biomass ranged more narrowly from 488 to 545 mg C m^{-2}, and was comprised of 60% dinoflagellates, 30% other flagellates and 11% ciliates. Nano-sized (<20 μm) protists accounted for the majority (57%) of grazer biomass and were positively correlated with picoplankton, partially supporting our hypothesis, but nanoplankton and micro-grazers (>20 μm) were not significantly correlated. The relative constancy of H-protist biomass among locations despite clear changes in integrated autotrophic biomass, Chl *a*, and primary production suggests that mesozooplankton may exert a tight top-down control on micro-grazers. Biomass-specific consumption rates of phytoplankton by protistan grazers suggest an instantaneous growth rate of 0.52 day^{-1} for H-protists, similar to the growth rate of phytoplankton and consistent with a trophically balanced ecosystem dominated by pico-nanoplankton interactions.

KEYWORDS: heterotrophic protists; microzooplankton; nanozooplankton; community composition

available online at www.plankt.oxfordjournals.org

INTRODUCTION

The Costa Rica Dome (CRD) is a 300- to 500-km open-ocean upwelling region in the Eastern Tropical Pacific centered around 9°N, 90°W (Wyrtki, 1964; Fiedler, 2002). Shoaling of the thermocline ridge is strongest during summer and results in seasonally high chlorophyll *a* (Chl *a*) concentrations (Fiedler, 2002). Despite a shallow thermocline and enhanced nutrient concentrations in the region, the CRD is distinct from other upwelling areas in the dominance of small picophytoplankton, specifically *Synechococcus* (Li *et al.*, 1983), as opposed to larger phytoplankton such as diatoms. Trace metal experiments suggest that limitation by cobalt, iron or zinc contribute to the dominance of such small primary producers in this otherwise high-nutrient environment by limiting the growth of larger phytoplankton (Franck *et al.*, 2005; Saito *et al.*, 2005; Ahlgren *et al.*, 2014).

Protistan grazers are important consumers in pelagic food webs, responsible for grazing the majority of global primary production (Calbet and Landry, 2004; Calbet, 2008) and playing key roles as nutrient recyclers and trophic links to larger zooplankton (Stoecker and Capuzzo, 1990; Sherr and Sherr, 2002; Sommer *et al.*, 2002; Calbet and Saiz, 2005). Microzooplankton grazers are abundant in both open-ocean (Lessard and Murrell, 1996; Pasulka *et al.*, 2013) and upwelling regions (Chavez *et al.*, 1996; Taylor *et al.*, 2011; Linacre *et al.*, 2012), although taxonomic dominance within the assemblages varies with location and size structure of phytoplankton prey. Heterotrophic dinoflagellates (H-Dino) and ciliates (Cil) generally dominate microzooplankton biomass in eutrophic upwelling regions associated with larger primary producers (Sherr and Sherr, 2007; Calbet, 2008; Linacre *et al.*, 2012), while heterotrophic nanoflagellates (H-Flag) are more important in oligotrophic open-ocean areas associated with small picophytoplankton (Lessard and Murrell, 1996; Calbet, 2008). Because the CRD is a unique upwelling region dominated by small primary producers, small heterotrophs in the microbial loop, including heterotrophic prokaryotes (H-Bact) and eukaryotic nano- (2–20 μm) and microzooplankton (20–200 μm) grazers, are expected to play key roles in mediating trophic interactions in the region. This has important implications for energy transfer efficiencies due to the 50–70% energy loss with each trophic step (Straile, 1997). Characterizing the heterotrophic microbial community of the CRD is therefore integral to understanding trophic interactions and energy flows within the region.

To date, only two studies have reported significant data on the heterotrophic community of the CRD. As part of the EASTROPAC program in the late 1960s, Beers and Stewart (Beers and Stewart, 1971) estimated protistan biovolumes and inferred microzooplankton grazing rates from samples collected in the CRD region. However, their results were limited to Cil and less abundant acantharians because H-Dino and H-Flag were not distinguishable by the techniques of that time. More recently, Olson and Daly (Olson and Daly, 2013) provided a modern and rigorous analysis of heterotrophic protist (H-protist) biomass and a few grazing estimates for a late-autumn CRD cruise, but supporting data were insufficient for assessing structural and rate relationships.

The CRD FLUx and Zinc Experiments (FLUZiE) cruise in June–July 2010 provided an opportunity to examine composition and biomass of the heterotrophic microbial community within the context of a broader food-web study (Landry *et al.*, 2016a) and during summertime, when thermocline shoaling is typically at its maximum. Since picophytoplankton biomass is known to be high in the CRD, we hypothesized that predator–prey pairs would be tightly associated (i.e. picoplankton consumed by nano-grazers, and in turn by micro-grazers) and readily apparent within the biomass size structure of the auto- and heterotrophic microbial community. Using community composition and biomass with experimental rate estimates from companion studies (Selph *et al.*, 2016), we also infer growth rate relationships for H-protist and compare our findings with recent predictions that mixotrophy should dominate as a trophic strategy among protists in open-ocean ecosystems.

METHOD

Study design and sampling

Cruise sampling in the CRD was done on *R/V Melville* from 22 June –27 July 2010 during five multi-day, semi-Lagrangian experiments, referred to as cycles. During each cycle, sampling and daily *in situ* incubation experiments were conducted while following a satellite-tracked drifter with a holey-sock drogue centered at 15 m (Landry *et al.*, 2009, 2016a). Of the five experimental cycles, the first was located close to the Costa Rica coast and outside of the CRD, so only Cycles 2–5 are considered here (Fig. 1). Seawater samples were collected from eight depths within the euphotic zone on each night of the cycles, from 2 m to 80–100 m depending on the fluorescence profiles from the CTD. Seawater was collected from Niskin bottles using silicone tubing and preserved as described below for each analysis.

Microscopic analysis of water-column samples

Seawater samples of 500 mL were preserved for epifluorescence microscopy with 260-μL alkaline Lugol's solution,

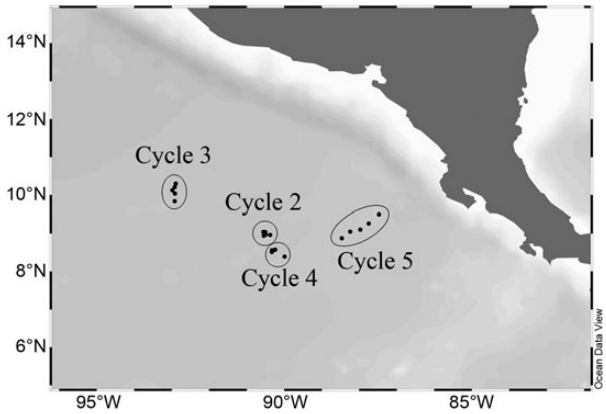

Fig. 1. Map of study region, including cruise sampling locations for Cycles 2–5.

10-mL buffered formalin, 500-mL sodium thiosulfate and 1-mL proflavin (0.033% w/v) (Sherr and Sherr, 1993). Preserved samples were allowed to sit for 1 h in the dark, then stained with 1-mL DAPI (0.01 mg mL^{-1}) before filtration. Aliquots of 50 mL were filtered onto 25-mm, 0.8-μm black polycarbonate membranes for the analysis of small cells, and the remaining 450 mL was filtered onto 25-mm, 8.0-μm black polycarbonate membranes. Membrane filters were mounted on glass slides using Type DF immersion oil, No. 2 glass coverslips, and stored at −80°C until analysis. Slides were imaged and digitized on a Zeiss AxioVert 200 M inverted epifluorescence microscope with motorized stage. Images were captured with a Zeiss AxioCam MRc black and white camera, utilizing separate filter sets for Chl *a*, DAPI, FITC and phycoerythrin. Slides with 0.8- and 8.0-μm membrane filters were imaged at ×630 and ×200, respectively.

At each image location, 7 z-stack images were taken. The z-stack images were processed and combined using the ImagePro software, and a fast Fourier transform and Laplace filter were applied to reduce the halo effect around cells. Counting and sizing of cells was also done with the ImagePro software. Cells were manually identified and grouped into functional groups: H-Dino and H-Flag discussed in this paper, as well as autotroph populations discussed in Taylor *et al.* (Taylor *et al.*, 2016). H-Dino included cells that could be positively identified as dinoflagellates by the presence of a clear dinokaryon, two flagella and an obvious theca for thecate forms. H-Flag included other heterotrophic cells that were largely flagellated but otherwise unidentifiable. Cells were binned into size categories based on the longest cell axis: <2, 2–5, 5–10, 10–20, 20–40 and >40 μm. Cell biovolumes (μm^3) were calculated using length and width measurements in the formula for a prolate sphere ($BV = 0.524 \times L \times W^2$). Carbon biomass was calculated from biovolumes as: pg C $cell^{-1} = 0.216 \times BV^{0.939}$ for non-diatoms and pg C $cell^{-1} = 0.288 \times BV^{0.811}$ for diatoms (Menden-Deuer and Lessard, 2000). More detailed information on the epifluorescence methods are in Taylor *et al.* (Taylor *et al.*, 2016). Biomass was depth-integrated according to the trapezoidal rule, averaging community biomass between sampling depths and summing biomass contributions for all depth strata (to the deepest depth sampled for each cycle; Fig. 2).

Seawater samples of 125 mL were also preserved with 5% acid Lugol's solution in amber bottles for the analysis of Cil by transmitted light microscopy. Prior to filtration, 37% formaldehyde was added to the sample (2% final concentration) and allowed to fix for 12 h to solidify cell membranes. Samples were filtered onto 25-mm, 8.0-μm polycarbonate membranes under low pressure (<50 mmHg), and the vacuum pump was shut off during the final few milliliters to allow for gentle gravity filtration. Filters were briefly placed on plain paper to wick away residual moisture, mounted on glass slides using Cargille immersion oil A (Certified Refractive Index Liquids, $n_D^{25°C}$ 1.584 ± 0.0002), and coverslips were sealed with clear nail polish (Freibott *et al.*, 2014). The slides were imaged and processed as described above for epifluorescence microscopy.

Cil were divided into broad taxonomic groups, including aloricate oligotrichs and choreotrichs, tintinnids, scuticociliates, cyclotrichs and other unidentifiable Cil (Agatha, 2004). Large mixotrophic oligotrichs of the genus *Tontonia* were clearly recognizable in the samples and quantified separately. Cells were binned by size based on the longest cell dimension: 8–20, 20–40 and >40 μm. Due to the pore size of the filter used, most nano-sized Cil likely passed through the membrane and are not accounted for here. Length and width measurements from each cell were used to calculate cell biovolume based on the most appropriate cell shape: prolate spheroid ($BV = 0.524 \times L \times W^2$), cone ($BV = 0.262 \times L \times W^2$) or cone plus half sphere [$BV = 0.262 \times W^2 \times (L + W)$]. Carbon biomass was calculated from cell biovolume as pg C = 0.19 × BV (Putt and Stoecker, 1989). Both Cil and dinoflagellates were manually counted in acid Lugol's samples; however, autotrophic and H-Dino are indistinguishable when stained with acid Lugol's fixative, so only epifluorescence estimates of H-Dino abundance and biomass are used in this analysis.

Additionally, at a single station in each cycle, 10–40 L of seawater from six to seven depths was collected for separate analyses of rare tintinnid Cil. Samples were not collected on the same casts or depths as those for microscopy described above, so they are treated here as a separate dataset. Samples were immediately concentrated to 100 mL using a 20-μm mesh and preserved with 2% acid Lugol's. They were then pipetted into Utermöhl (Utermöhl, 1931) settling chambers, settled for 12–24 h, and counted on an

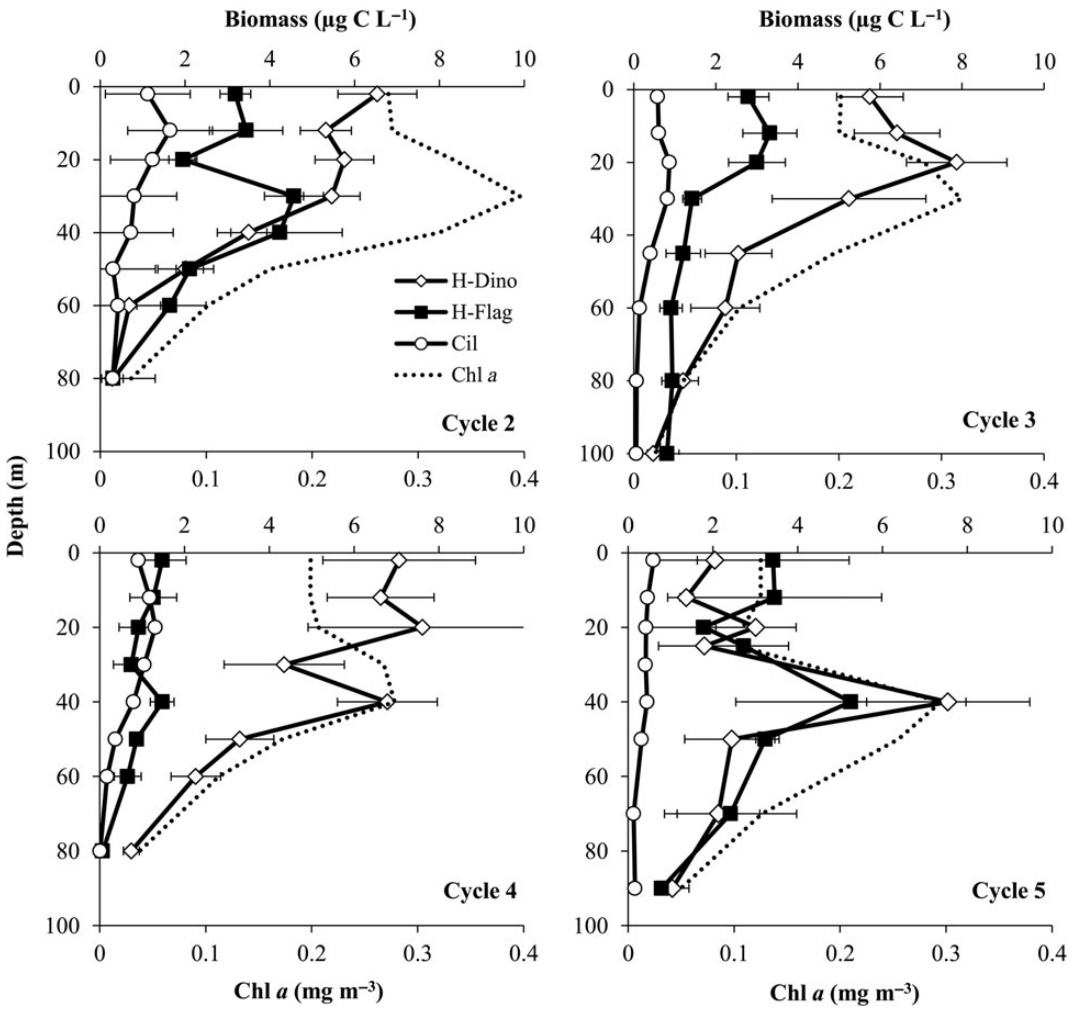

Fig. 2. Depth profiles of mean total biomass (µg C L^{-1}) for all heterotrophic dinoflagellates (H-Dino) and heterotrophic flagellates (H-Flag) from epifluorescence microscopy and ciliate biomass (Cil) from transmitted light microscopy. Dotted line and secondary *x*-axis show mean chlorophyll concentration (mg Chl *a* m^{-3} = µg Chl *a* L^{-1}). Biomass was averaged over the 4-day cycles to obtain mean and standard error bars for each cycle ($n = 5$ for Cycle 2–4; $n = 2$ for Cycle 5).

Olympus IX 71 inverted microscope at ×200 or ×400. Individual cells were photographed, measured and identified to species (Kofoid and Campbell, 1929, 1939; Marshall, 1969; Zhang *et al.*, 2011). All loricae were measured for length and width, and cell biovolumes were calculated and converted to carbon biomass using the equation, pg C = 0.053 × BV (Verity and Langdon, 1984).

Flow cytometry analysis

Seawater samples (1 mL) were preserved with 0.5% paraformaldehyde (v/v, final concentration), flash frozen in liquid nitrogen and stored at −80°C. Prior to analysis, samples were thawed and stained with Hoechst 34 442 (1 µg mL^{-1}) for 1 h in the dark (Monger and Landry, 1993). Aliquots of 100 µL were analyzed using a Beckman-Coulter EPICS Altra flow cytometer with a Harvard Apparatus syringe pump for volumetric sample delivery and two argon lasers tuned to UV (200 mW) and 488 nm (1 W) excitation. Fluorescence signals were collected using filters for Hoechst-bound DNA (blue fluorescence, 450 nm), phycoerythrin (orange fluorescence, 575 nm) and Chl *a* (red fluorescence 680 nm), and normalized to external standards of 0.5 µm yellow-green and 0.5 µm UV polystyrene beads. Cell fluorescence and light-scatter properties were acquired with the Expo32 software and subsequently analyzed with the FlowJo software to define H-Bact populations based on DNA signal (all living cells), absence of photosynthetic pigment and light-scatter signals (forward and 90°light scatter, measures of relative size).

Abundance estimates of H-Bact from flow cytometry analysis were converted to carbon biomass using carbon per cell conversions and depth, using bead-normalized forward angle light scattering (FALS) as a relative measure

of cell biovolume (Linacre *et al.*, 2010, 2012). Estimates of cell carbon content were made using an open-ocean, mixed layer estimate of 10 fg C cell^{-1} as a starting point for H-Bact (Garrison *et al.*, 2000). Then, using the scaling factor FALS$^{0.55}$ (Binder *et al.*, 1996), the carbon:cell content was determined for each depth from the specific mean cell carbon values and the FALS ratio (FALS$_{sample}$:FALS$_{mean}$)$^{0.55}$.

Trophic relationships

We examined potential relationships among autotrophic and heterotrophic size classes using Pearson correlations for biomass values in the upper 45 m, a depth range that includes the mixed layer and chlorophyll maximum on all cycles and accounts for >93% of the primary production (Landry *et al.*, 2016b). Correlations between predator–prey pairs were expected to be negative (e.g. Schmoker and Hernández-León, 2013), indicative of Lotka–Volterra-style oscillations and significant top-down grazer impacts. However, previous studies have also found positive correlations between presumptive predators and prey (Hwang and Heath, 1997; Yang *et al.*, 2008), which may be indicative of strong bottom-up forcing and rapid response of protistan consumers to prey dynamics.

We also used the relationship between the carbon consumed by microzooplankton grazing and H-protist biomass to derive biomass-specific estimates of carbon consumption and growth rate potential of the H-protist assemblages. For these analyses, phytoplankton growth rates and mortality losses to microzooplankton grazing were determined from results of *in situ* incubated dilution experiments (Landry *et al.*, 2016b; Selph *et al.*, 2016). Briefly, during each 4-day experimental cycle, two-treatment dilution experiments were conducted daily at eight depths spanning the euphotic zone, with *in situ* bottle incubations attached to the surface drifter. Experiments were set up with water from the same depths and CTD casts as the samples for community analysis. We used the instantaneous rates of growth and grazing mortality from these experiments along with the corresponding estimates of total autotroph carbon from flow cytometry and microscopy (Taylor *et al.*, 2016) to compute carbon-based grazing rate impacts on the phytoplankton community from the equations in Landry *et al.* (Landry *et al.*, 2000).

RESULTS

Environmental conditions of the sampling sites

Table I gives the dates, locations, euphotic zone depth and mean mixed-layer characteristics for the five experimental cycles conducted on the cruise, and the relative positions of the cycles and daily sampling points are shown in Fig. 1. Physical circulation and hydrographic features of the sampling sites are fully described by Landry *et al.* (Landry *et al.*, 2016a), and detailed presentations of profiled properties are presented elsewhere (Selph *et al.*, 2016; Taylor *et al.*, 2016). Cycle 1, conducted in southward flowing waters close to the Costa Rica coast, is not included in the present analysis. Cycle 2 sampled in the central dome area ~9°N, 91°W, which was located by a transect survey. At the end of Cycle 2, we deployed a satellite-tracked surface drifter with a mixed-layer drogue, and relocated later as the starting point for Cycle 4. In the meanwhile, Cycle 3 was done in waters northwest of the dome. Cycle 5 was conducted east of the dome region in North Equatorial Counter Current (NECC) waters flowing rapidly toward the coast. Several connections can be made among the experiments based on study design and subsequent hydrographic analysis. Cycles 2 and 4 were clearly in the central dome region, and Cycle 3 also fits the criterion for being in the dome region, with the 20°C isotherm at ≤35 m (Fiedler, 2002). Cycle 5 was located out of the dome region, but had T-S properties closely resembling Cycle 4 (Landry *et al.*, 2016a).

Table I: Sampling dates, initial locations, euphotic zone depth (1% surface irradiance) and mean mixed-layer characteristics for experimental Cycles 1–5

					Mixed layer characteristics		
Experiment	Dates	Lat (°N)	Lon (°W)	1% Io (m)	MLD (m)	*T* (°C)	NO_3 (μM)
Cycle 1	23–27 June	9.72	87.00	45.9	23.8	28.4	0.09
Cycle 2	4–8 July	9.04	90.56	44.6	18.7	25.5	6.9
Cycle 3	9–13 July	10.42	92.92	52.1	21.1	27.3	3.1
Cycle 4	15–19 July	8.55	90.40	49.7	20.5	26.0	5.2
Cycle 5	20–24 July	8.88	88.46	56.7	30.9	27.3	2.7

Dates are local time, with daily early morning CTD casts at ~0200. Mixed layer depth (MLD) = depth at which density exceeds 0.05 kg m^{-3} of surface value).

Hydrocast profiles for all cycles showed strong stratification of temperature, oxygen and nutrients. The central dome region (Cycles 2 and 4) had the shallowest mixed layers (19 and 21 m, respectively), the lowest mean mixed-layer temperature (25.5–26°C) and the highest concentration of mixed-layer nitrate (5–7 μM, Table I). At all sampling locations, however, temperature decreased sharply by 10°C or more in the upper 50 m, which comprised all or most of the euphotic zone at all locations. Oxygen concentrations declined by almost an order of magnitude and nitrate increased by 25 μM over the same depth range.

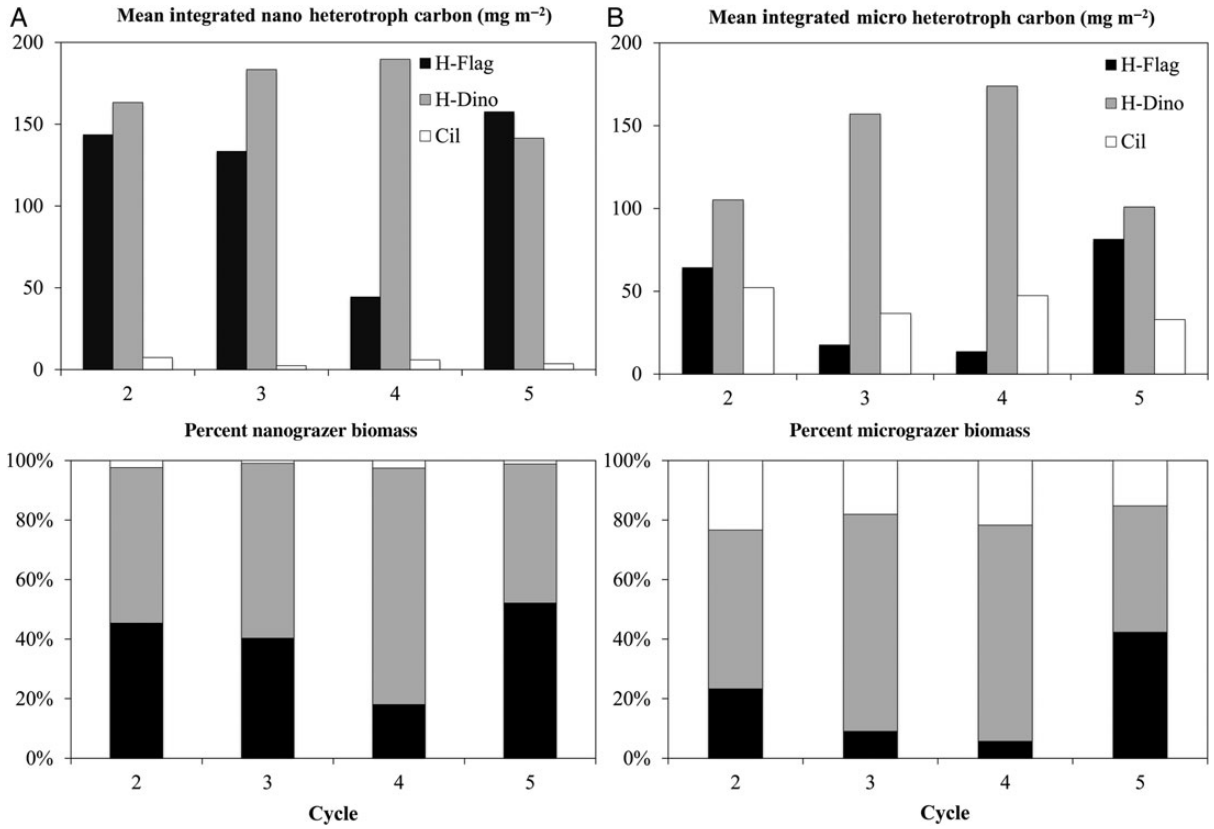

Fig. 3. Mean total integrated grazer biomass (mg C m^{-2}) and percentage of total biomass, including heterotrophic flagellates (H-Flag), heterotrophic dinoflagellates (H-Dino) and ciliates (Cil). Grazers were separated into (**A**) nano (2–20 μm) and (**B**) micro (20–200 μm) size classes, integrated with depth for each day of the experimental cycle and averaged over the 5 sampling days for each cycle.

Heterotrophic dinoflagellates and flagellates

H-Dino and other unidentified flagellates (H-Flag) constituted the majority of micro-grazer biomass in the CRD, averaging 59 and 31%, respectively, across all cycles. Mean H-Dino + H-Flag biomass was greatest at or above the chlorophyll maximum for all cycles (1.5–7.9 μg C L^{-1}) although Cycle 5 exhibited the most pronounced peak at the 40-m chlorophyll maximum (7.5 and 5.3 μg C L^{-1}, respectively). H-Dino biomass generally exceeded H-Flag biomass during Cycles 2–4. However, H-Flag biomass was approximately the same as H-Dino and at times dominated biomass below 30 m in Cycle 2 and throughout the water column in Cycle 5 (Fig. 2).

Across all cycles, integrated H-Flag biomass was comprised of 39% nano-sized cells and 20% micro-sized cells. Cycle 5 had the highest mean integrated biomass of H-Flag (158 and 81 mg C m^{-2} for nano- and micro-sized H-Flag, respectively; Fig. 3). Cycle 4 had the lowest H-Flag biomass (44 and 14 mg C m^{-2} for nano- and micro-sized H-Flag, respectively). H-Dino integrated biomass was evenly distributed between nano- (59%) and micro-grazer (60%) size classes across all cycles. Mean integrated biomass of H-Dino was greatest for Cycle 4 (190 and 174 mg C m^{-2} for nano and micro H-Dino, respectively). Cycle 5 had the lowest H-Dino integrated biomass (142 and 101 mg C m^{-2} for nano and micro H-Dino), illustrating that biomass of H-Dino did not vary as dramatically as H-Flag biomass across cycles. Mean abundances and biomasses of H-Flag, H-Dino, Cil and H-Bact at each sampling depth are given in Supplementary Data, Table SI.

Although the above estimates of H-Dino biomass were obtained from analyses by epifluorescence microscopy, dinoflagellates were also noted in the acid Lugol's preserved samples. The trophic status of these dinoflagellates could not be determined by transmitted light microscopy, so these observations are qualitative rather than quantitative. In these samples, dinoflagellates were dominated by athecate, gymnodinoid forms, such as *Gyrodinium*, which are typically heterotrophic. Other notable dinoflagellate taxa included *Oxytoxum* and *Protoperidinium*, both with known heterotrophic species (Olseng *et al.*, 2002; Mertens *et al.*, 2013; Barton *et al.*, 2013). The composition agrees well with the only other reported data for the region (Olson and Daly, 2013), which found that 26–43% of

total dinoflagellates were heterotrophic gymnodinoids and identified protoperidinoids in a few sampling locations.

Ciliate biomass and taxonomic distribution

Ciliate biomass was highest in Cycles 2 and 4, which were situated closest to the dome center (Landry *et al.*, 2016a). With the exception of Cycle 5, which had the lowest overall ciliate biomass and the least discernable water-column variation, ciliate biomass was highest at or above the chlorophyll maxima (range 0.18–0.48 mg Chl *a* m^{-3}, mean 0.34 mg Chl *a* m^{-3}), which fell between 20 and 40 m in all cycles (Fig. 2).

Mean integrated ciliate biomass was 50.7 mg C m^{-2}, varying considerably from 85 mg C m^{-2} in Cycle 2 to 28.6 mg C m^{-2} in Cycle 5. Despite the cycle differences in total ciliate biomass, taxonomic composition varied little and was dominated by aloricate oligotrichs (mean 75%, range 72–77% of ciliate biomass across cycles). Tintinnids constituted 10–18% of total ciliate biomass (mean = 13%), and Cil categorized as other or unidentifiable averaged 11% of total biomass. The latter category contained a very small number of scuticociliates and cyclotrichs, but the majority were likely aloricate oligotrichs that had been damaged in processing and could not be classified.

A separate analysis of tintinnid species and abundance collected from larger 10–40 L samples yielded further information on ciliate diversity in the CRD. Of the 40 species identified, the three most numerous species were *Ascampbelliella armilla*, *Acanthostomella obtusa* and *Dadayiella ganymedes*, which exceeded total abundances of 20 cell L^{-1} and constituted 54% of tintinnids in all samples. For further details on the tintinnid species, see Supplementary Data, Fig. S1. The pattern of tintinnid biomass from this separate sampling method agrees with the acid Lugol's analyses of total ciliate biomass, which found the greatest percentage of integrated tintinnid biomass in Cycles 5 (18%) and 2 (14%), and the lowest in Cycles 3 and 4 (both 10%). Additionally, the mean oral diameters of the cell loricae (Dolan, 2012) suggest that 60–90% of CRD tintinnids should feed most efficiently on nano-sized prey with preferred spherical diameters between 7 and 10 μm, supporting our expectation of a potential predator–prey relationship between Cil and nano-sized prey.

Some groups of Cil displayed specific patterns among cycles. Known ciliate mixotrophs in the genus *Tontonia* were most abundant in Cycle 5. Although this cycle had the lowest total ciliate biomass, it had the highest presence of *Tontonia* on multiple sample days and depths, comprising 96% of total ciliate biomass in one surface sample. *Tontonia* were noted multiple times, but to a lesser extent, in Cycles 3 and 4, and were not present in Cycle 2 samples, closest to the dome center. Scuticociliates, known to be bacterivores, were mainly present in Cycle 2 in small numbers typically comprising less than 10% of total ciliate biomass. Cyclotrichs, such as the mixotrophic *Mesodinium*, were also very rare but present during Cycle 2.

Most Cil (90%) fell into the micro-grazer size category, with only a small number of nano-Cil (Fig. 3). Across all cycles, integrated nano-ciliate biomass averaged only 2% of total nano-grazer biomass, whereas micro-sized Cil averaged 20% of micro-grazer biomass (Fig. 3). It should be noted that Cil smaller than 8–10 μm would have been missed entirely due to the 8-μm pore size of the membrane filter used in this analysis, so numbers of nano-ciliates should be considered underestimates. However, the only previously reported data on Cil in the Eastern Tropical Pacific (Olson and Daly, 2013) indicate that Cil less than 20-μm account for less than 15% of total grazer biomass, and even less (<10%) at stations within the CRD. Thus, the <10-μm Cil missed by our methods likely comprise a very small percentage of the total biomass.

Heterotrophic bacteria

Mean integrated H-Bact biomass was highest in Cycle 2 (487 mg C m^{-2}) and lowest in Cycle 4 (180 mg C m^{-2}; Fig. 4B). Significant linear relationships (Model II linear regression, reduced major axis) were found between H-Bact biomass and total autotrophic carbon biomass (Fig. 4A, $Y = 0.16X - 0.37$, $r^2 = 0.54$, $P < 0.0001$), primary production ($Y = 0.21X + 0.17$, $r^2 = 0.27$, $P < 0.0001$) and Chl *a* ($Y = 28.2X - 1.9$, $r^2 = 0.16$, $P < 0.0001$). However, the goodness of fit between H-Bact biomass and Chl *a* or primary production were substantially lower than between H-Bact and autotroph carbon biomasses.

Size class comparisons and carbon biomass relationships

As seen in Fig. 3, mean integrated biomass of nano-grazers exceeded micro-grazers in all cycles, with highest values in Cycles 3 (319 mg C m^{-2}) and 2 (314 mg C m^{-2}). Micro-grazer biomass was highest in Cycle 4 (235 mg C m^{-2}), which had nearly equal distributions between nano- (240 mg C m^{-2}) and micro-size classes. Total depth-integrated biomass of H-protists (H-Dino, H-Flag and Cil) varied little across cycles, ranging from 536 mg C m^{-2} in Cycle 2 to 488 mg C m^{-2} in Cycle 4 (Fig. 4B). Ratios of total autotrophic carbon (Taylor *et al.*, 2016) to total H-protist carbon varied from 5.1 in Cycle 2–2.7 in Cycle 5.

Depth-integrated H-protist carbon correlates positively with carbon of micro-sized autotrophs (Pearson's correlation, $r = 0.68$, $P < 0.01$), but not with nano- or picoautotrophs. Integrated microheterotroph biomass also positively correlates with microautotroph carbon ($r = 0.58$, $P < 0.05$).

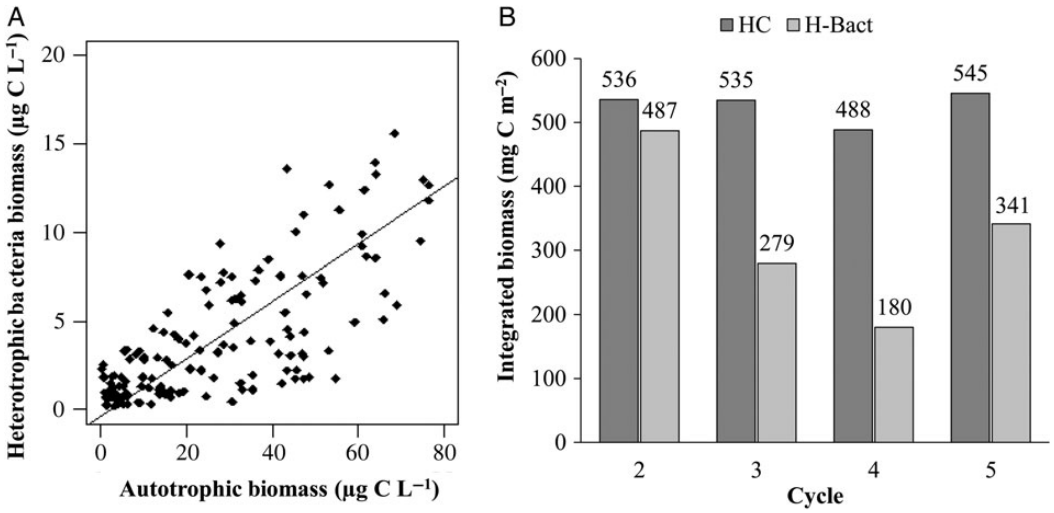

Fig. 4. (**A**) Total biomass (µg C L^{-1}) of all autotrophs determined by epifluorescence microscopy and heterotrophic bacteria (H-Bact) determined by flow cytometry shows a significant linear regressions ($y = 0.16x - 0.37$, $R^2 = 0.54$, $P < 0.0001$). (**B**) Total integrated heterotrophic protist biomass (H-Prot, mg C m^{-2}) including H-Dino, H-Flag and Cil biomass, compared with integrated heterotrophic bacterial biomass (H-Bact, mg C m^{-2}).

Integrated nanoautotroph carbon is positively correlated with H-Flag biomass ($r = 0.68$, $P < 0.01$) and negatively with H-Dino biomass ($r = -0.63$, $P < 0.01$), suggesting grazing by H-Dino on nano-autotrophs.

H-Nanos are significantly correlated with picoplankton ($r = 0.33$, $P < 0.01$), and significant correlations between H-Nanos and both *Synechococcus* ($r = 0.34$, $P < 0.01$) and H-Bact ($r = 0.31$, $P < 0.01$) suggest grazing on these specific pico-sized groups. H-Micros are not significantly correlated with any potential prey size group, suggesting top-down control on this group specifically.

Heterotrophic protist biomass and grazing relationships

The slope of the regression relationship between total H-protist carbon biomass and the carbon consumed by microzooplankton grazing (2.3 µg C µg C L^{-1} day^{-1}; $P < 0.0001$; Fig. 5) provides an estimate of the mean biomass-specific grazing rate of H-protists in the CRD, in this case, 230% body C consumed day^{-1}. This is a conservative estimate of total protistan phagotrophy because it considers only phytoplankton prey and neglects likely feeding on H-Bact and other H-protists (e.g. Cil or H-Dino feeding on nano-heterotrophs) or consumption of detrital particles. Assuming a gross growth efficiency of 30% for H-protists (Straile, 1997; Landry and Calbet, 2004), phytoplankton consumption must therefore support at least a daily mean growth equivalent to 69% of biomass, which translates to an instantaneous growth rate of 0.52 day^{-1}. This computed rate is very similar to the measured integrated instantaneous growth rate of phytoplankton, 0.56 d^{-1}, determined by the dilution experiments conducted on the cruise (Landry *et al.*, 2016b).

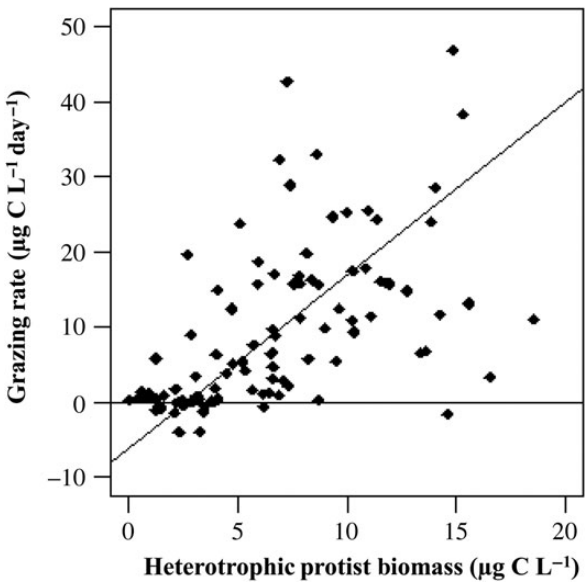

Fig. 5. Linear regression (Model II, reduced major axis) of microzooplankton grazing rates (µg C L^{-1} day^{-1}) determined from dilution experiments as described in Landry *et al.* (Landry *et al.*, 2016b) with heterotrophic protist biomass (µg C L^{-1}) ($y = 2.3x - 6.13$, $R^2 = 0.56$).

DISCUSSION

This study constitutes the first dataset of sufficient sample size and scope to explore the size structure and

composition of the heterotrophic microbial community in the CRD relative to contemporaneous estimates of autotrophic carbon, bacterial carbon and grazing rates. When interpreting results, however, it is important to consider that summer 2010 was not typical of the region. Our cruise was preceded by moderate El Niño physical conditions in winter and spring. Although those conditions had diminished by mid-summer and were even reversing to La Niña-like in the latter half of the year, 2010 still stands out as the only year without a clear mid-summer elevation of surface Chl *a* in a decade of satellite observations from 2004 to 2014 (Landry *et al.*, 2016a). Concentrations of *Synechococcus*, while still high, were almost an order of magnitude lower during our cruise compared with abundances reported previously (Li *et al.*, 1983; Saito *et al.*, 2005). Since normal summertime characteristics of the phytoplankton community in the dome were likely suppressed in 2010, it is reasonable to expect that both the autotroph and heterotroph microbial assemblages would have been sampled at unusually low seasonal levels. Thus, the trophic relationships from this study may be more informative than the absolute magnitudes observed.

CRD protistan grazer composition and comparisons

Nano-sized grazers dominate biomass across the CRD region, specifically small H-Dino. Since picophytoplankton, such as *Synechococcus*, comprised the majority of phytoplankton biomass measured (Landry *et al.*, 2016b; Taylor *et al.*, 2016), it was expected that nano-sized protists would likely dominate as grazers. It is notable, however, that H-Dino are important in CRD waters, where diatoms are scarce (~1% of phytoplankton biomass; Taylor *et al.*, 2016), because H-Dino are often seen in association with diatoms due to their ability to feed on cells as large, or larger, than themselves (Naustvoll, 2000; Sherr and Sherr, 2007). In the CRD, therefore, the importance of H-Dino is indicative of their broader trophic role as consumers, as opposed to diatom specialists.

In comparing our results to previous analyses of H-protists in open-ocean areas of the Eastern Tropical Pacific (Table II), it is clear that flagellate biomass, including H-Dino, usually exceeds that of Cil. The findings of Verity *et al.* (Verity *et al.*, 1996) from US JGOFS studies in the equatorial upwelling region at 140°W stand out as an extreme in this regard, with very low ciliate biomass and dominance of H-Flag over H-Dino. Other studies with data in the same area, however, show a general pattern in which Cil, H-Flag and H-Dino all comprise significant components of the grazer assemblage (Chavez *et al.*, 1996; Taylor *et al.*, 2011). In fact, the overall taxonomic divisions of biomass among H-Dino, H-Flag and Cil in the heterotrophic community studied by Yang *et al.* (Yang *et al.*, 2004) and Olson and Daly (Olson and Daly, 2013) are very similar to that found in this study: H-Dino dominate heterotrophic biomass while H-Flag and Cil make up sizable fractions (10–40%) depending on location and depth.

Our results are most directly comparable with that of Taylor *et al.* (Taylor *et al.*, 2011) based on the same methods used for sample preservation and epifluorescence microscopy, and with that of Olson and Daly (Olson and Daly, 2013) based on the area sampled. In comparison with the former, we found higher absolute and relative contributions of flagellates generally, H-Dino in particular, in the CRD relative to the equatorial upwelling system (Taylor *et al.*, 2011). For Cil, the highest biomass measured in the CRD is similar to the mean euphotic zone values measured in the equatorial upwelling region (3.4 vs. 2.9 $\mu g\ C\ L^{-1}$, respectively). As noted previously, it is possible, though unlikely, that we missed a large enough biomass of nano-sized Cil by using an 8-μm pore filter in our slide preparation procedure to account for significant system differences, and low Cil concentrations in equatorial upwelling waters have also been reported (Verity *et al.*, 1996). Another explanation for lower mean Cil values in our CRD results is that we analyzed samples taken much deeper in the water column (80–100 m) than the depths of significant primary productivity (93% occurred above 40 m; Landry *et al.*, 2016b). Nonetheless, when results are compared on an areal basis, the differences are clear. The highly stratified and shallow euphotic zone of the CRD had higher integrated biomass of H-protists on average compared with that in the deep euphotic zone of the equatorial upwelling region (525 and 368 $mg\ C\ m^{-2}$, respectively), and the partitioning among H-Flag, H-Dino and Cil groups was substantially different between these studies.

On average, total heterotrophic biomass in the equatorial Pacific study was evenly divided between flagellates, including both H-Flag and H-Dino groups, and Cil (53 and 47%, respectively; Taylor *et al.*, 2011), compared with the clear dominance of flagellates in the CRD (90% H-Dino and H-Flag vs. 11% Cil). Mean mixed-layer Chl *a* concentrations (0.2–0.3 $mg\ m^{-3}$) were similar between regions, as were mean estimates of depth-integrated autotrophic biomass (1390 $mg\ C\ m^{-2}$ for the CRD and 1385 $mg\ C\ m^{-2}$ for the equatorial Pacific; Taylor *et al.*, 2011, 2016). Thus, it appears that seemingly small, but important, differences in phytoplankton community composition can substantially impact the composition of co-occurring H-protists. Picophytoplankton clearly dominated CRD biomass (60 vs. 39% in equatorial Pacific; Taylor *et al.*, 2016), whereas nanoplankton accounted for the most biomass in the equatorial Pacific (Taylor *et al.*, 2011). Closer comparison shows that different taxa were more prominent

Table II: Comparison of heterotrophic protist biomass (μg C L^{-1}) reported in multiple studies across the equatorial and eastern Tropical Pacific Ocean

Region and protists	Location	Date	Biomass (μg C L^{-1})	References
Eastern Tropical Pacific	10°N–12°S, 105°W	February–April 1968		Beers and Stewart (1971)
Ciliates			0.13–0.76	
Equatorial Pacific				
Heterotrophic flagellates	10°N–8°S, 110°W	Spring 1992	1.4 ± 0.5	Vørs *et al.* (1995)
Choanoflagellates	and 8°S–12°N, 125°W		0.1 ± 0.1	
Heterotrophic dinoflagellates			3.0 ± 1.5	
Ciliates			1.0 ± 0.7	
Equatorial Pacific upwelling				
<20 μm flagellates	0°, 140°W	February–April 1992	6	Verity *et al.* (1996)
Heterotrophic dinoflagellates		August–October 1992	1.3	
Ciliates			0.08	
<20 μm flagellates			5.9	
Heterotrophic dinoflagellates			1.8	
Ciliates			0.16	
Central and Eastern Tropical Pacific				
Heterotrophic flagellates	12°N–10°S, 95°W, 110°W,	Spring 1992	1.7 ± 1.3	Chavez *et al.* (1996)
Heterotrophic dinoflagellates	125°W, 140°W, 170°W	Fall 1992	2.3 ± 2.8	
Aplastic ciliates			1.5 ± 2.0	
Heterotrophic flagellates			1.5 ± 0.7	
Heterotrophic dinoflagellates			3.1 ± 0.5	
Aplastic ciliates			1.3 ± 1.4	
North Equatorial Pacific				
Heterotrophic flagellates	5°N–11°N, 130°30′W	July 1998	0.06–1.1	Yang *et al.* (2004)
Heterotrophic dinoflagellates			0.3–4.0	
Ciliates			0.03–2.9	
Equatorial Pacific upwelling				
Total heterotrophic protists	4°N–4°S,	December 2004,	1.5–8 (3.2)	Taylor *et al.* (2011)
Heterotrophic flagellates	110°W–140°W	September 2005	1.64	
Heterotrophic dinoflagellates			1.54	
Ciliates			1.4–2.9 (2.1)	
Eastern Tropical Pacific and CRD				
Heterotrophic flagellates	9°N–14°N,	October–November 2007	0.5–10.8 (2.1)	Olson and Daly (2013)
Heterotrophic dinoflagellates	90°W–106°W		0.2–14.3 (2.2)	
Ciliates			0.1–18.8 (3.8)	
Costa Rica Dome				
Heterotrophic flagellates	6°N–10°N,	June–July 2010	0.02–9.7 (1.9)	This study
Heterotrophic dinoflagellates	87°W–93°W		0.04–14.1 (4.1)	
Ciliates			0.02–3.4 (0.7)	

Numbers in parentheses are mean values. Ciliate biomass for Beers and Stewart (Beers and Stewart, 1971) was converted from the reported average volume ($mm^3\ m^{-3}$) using the Putt and Stoecker (Putt and Stoecker, 1989) carbon conversion discussed in the Method section. Table was revised and updated from Yang *et al.* (Yang *et al.*, 2004).

in the picophytoplankton communities of the two areas (*Synechococcus* and picoeukaryotes in the CRD and *Prochlorococcus* in the equatorial Pacific). In addition, diatom biomass was an order-of-magnitude greater in the equatorial Pacific (2.9–8.4 mg C m^{-2}) than in the CRD (0.2–0.8 mg C m^{-2}; Taylor *et al.*, 2016). Such differences, notably more nano-sized phytoplankton and more diatoms in the equatorial Pacific, likely provided more of the preferred prey resources for Cil in equatorial waters than were available in the CRD during our study. The similarities in mean Chl *a* and total autotrophic biomass of these two upwelling areas therefore mask significant differences in size-related trophic dynamics and plankton community compositions.

Our results differ in several ways from the previous H-protist analyses in the CRD by Olson and Daly (Olson and Daly, 2013). For example, our estimates of total heterotrophic biomass are lower (535 vs. 686 mg C m^{-2}, respectively), but Olson and Daly (Olson and Daly, 2013) also reported much higher Chl *a* values (mean = 0.8, max = 1.8 μg Chl *a* L^{-1}) than measured during our sampling (mean = 0.2 μg Chl *a* L^{-1}; Taylor *et al.*, 2016). Thus, H-protist biomass during our cruise was lower in absolute terms but disproportionately higher relative to Chl *a* as an indicator of autotroph biomass. Olson and Daly (Olson and Daly, 2013) also reported a higher percentage of Cil than we found (30 vs. 11%, respectively). Although H-Dino accounted for the highest percentages of heterotrophic biomass in both studies (41 and 60%, respectively), H-Flag were less important and Cil much more important in the previous analysis (Olson and Daly, 2013). These compositional differences might also be reasonably attributed to

higher autotrophic biomass on the previous cruise, assuming that higher food concentration and proportionately more large prey would provide a better growth environment for Cil than conditions during our cruise. However, there was no size or compositional analysis of the autotrophic community from the Olson and Daly cruise to evaluate this possibility. Additionally, since Cil are often preferred prey of larger zooplankton, differences in grazing impact of mesozooplankton (top-down control) could be an alternate explanation for the differences in ciliate biomass and heterotroph community composition between the two studies.

Biomass and grazing relationships

H-Bact consumes dissolved organic material produced by autotrophic organisms; thus, it is expected that their biomass should strongly correlate with total autotrophic biomass, Chl *a* and primary production, as noted elsewhere (Azam *et al.*, 1983; Taylor *et al.*, 2011). The significant linear relationship between H-Bact and total autotrophic biomass (Fig. 4A) underlies clear trends among the cycles, where H-Bact biomass tracks variations in autotrophic biomass. In contrast, H-protist biomass did not display clear patterns across cycles. Biomass of nano-grazers and total picoplankton were positively correlated, suggesting a potential predator–prey relationship between these size classes and supporting our hypothesis, but no significant relationship was found between nano-sized protists and microheterotrophs (H-Micros). These relationships suggest that bottom-up forcing has a strong influence on bacteria and picoplankton and their H-Nano consumers, whereas other factors, potentially top-down predation by mesozooplankton, may more strongly influence the microheterotroph assemblage.

The relatively constant depth-integrated biomass of H-protists among all sampling locations (488–545 mg C m^{-2}; Fig. 4B) despite clear changes in the integrated autotrophic biomass (1089–1858 mg C m^{-2}; Taylor *et al.*, 2016), integrated H-Bact biomass (180–487 mg C m^{-2}; Fig. 4B), total Chl *a* (16–31 mg Chl *a* m^{-2}; Taylor *et al.*, 2016) and primary production rates (40–70 mg C m^{-3}; Selph *et al.*, 2016) supports the potential of top-down pressure from mesozooplankton. Temporal or spatial imbalances between growth and grazing of predator and prey could also create such a condition; however, microzooplankton grazing rates closely tracked phytoplankton growth rates in individual dilution experiments and balanced picophytoplankton production for the region as a whole (Gutiérrez-Rodríguez *et al.*, 2016; Landry *et al.*, 2016b). Figure 5 also suggests a reasonable relationship between variations in H-protistan biomass and grazing impact on phytoplankton, although there is clearly much unexplained variability that may reflect compositional variability in consumers and prey. Nonetheless, at least from an experimental perspective, the strong coupling observed between protistan biomass and grazing, and between grazing and phytoplankton growth, would seem to argue that predatory influences of higher trophic levels have a key role in explaining the relative constancy of H-protistan biomass among cycles (Fig. 4B).

This idea is further supported by a separate analysis, which found very uniform mesozooplankton biomass among cycles (4.86–5.37 g m^{-2}) despite substantial differences in size structure, composition, biomass-specific grazing rates and diel vertical migratory behavior (Décima *et al.*, 2016). For instance, copepods were abundant in all cycles, while euphausiids notably dominated during Cycle 2 (Décima *et al.*, 2016), near the dome center, where Cil biomass was highest and diatom production insufficient to support mesozooplankton (Taylor *et al.*, 2016). In fact, Cycle 2 had high productivity, but the highest dominance of picophytoplankton and the lowest direct feeding of mesozooplankton on phytoplankton of all cycles. This suggests particularly high mesozooplankton grazing impact on microzooplankton during this cycle, which could explain its similarity in H-protist biomass to other cycles despite conditions of high productivity and picophytoplankton abundance, which would favor elevated H-protist biomass. The observed prevalence of salps and appendicularians during Cycle 5 (Décima *et al.*, 2016), another area of high productivity, suggests that indirect competition for picophytoplankton prey could also influence standing stocks of H-protists, in addition to direct predatory pressure by mesozooplankton. In this case, the different composition of mesozooplankton in Cycle 5 might be related to the distinctly lower ciliate biomass in that area (Fig. 2), while not having much of an impact on total H-protist biomass. Since top-down pressure from mesozooplankton could reasonably have an important regulatory role in the CRD, the micro-mesozooplankton link would be an interesting and important area of focused future study.

Across all cycles, the instantaneous growth rate of H-protistan grazers computed from measured grazing impact on phytoplankton (0.56 day^{-1}) in dilution experiments is similar to the measured growth rate of phytoplankton (0.52 day^{-1}). Because autotrophs and H-protists are both the potential prey for mesozooplankton, the calculated ability of protistan consumers of phytoplankton to sustain growth rates similar to that of phytoplankton is central to maintaining a balance between production and grazing (Landry *et al.*, 2011). Thus, this agreement supports the idea that the CRD is a trophically balanced ecosystem (Landry *et al.*, 2016b). These growth rates are also consistent with microzooplankton providing a significant carbon flow

to mesozooplankton in the CRD (Décima *et al.*, 2016), where picophytoplankton dominate phytoplankton biomass and two thirds of primary production is consumed by protists (Landry *et al.*, 2016b).

Potential mixotrophic complications

Another factor that could influence trophic relationships in the CRD is mixotrophy, a strategy that is reasonably expected among flagellates competing against dominant picophytoplankton for limiting nutrients or trace elements (Unrein *et al.*, 2014). Although we did not specifically address mixed trophic functionality in this study, mixotrophs are common within prymnesiophyte, ciliate (Esteban *et al.*, 2010) and flagellate groups (Green, 1991; Stoecker, 1999), and a recent model suggests that mixotrophy should be the dominant strategy for nanoflagellates in steady-state oligotrophic systems (Mitra *et al.*, 2014). While the predictions of this model agree well with our data with respect to the very low biomass contribution of diatoms in the CRD (non-motile microautotrophs, Supplementary Data, Fig. S2), they differ in substantially underestimating the prevalence of H-Flag, at least according to our ability to distinguish plastidic from non-plastidic cells by epifluorescence microscopy. As also illustrated in Fig. 5, the measured grazing impact of protistan consumers is well correlated with biomass of non-plastidic cells (H-protists), leading to reasonable estimates of biomass-specific ingestion and growth rates. Thus, mixotrophy does not need be invoked to explain the biomass and rate relationships found in our study, though it may nonetheless be present and important.

As a comparative exercise, we roughly estimated the potential grazing-equivalent biomass of mixotrophs in the CRD based on experimental results from the Equatorial Pacific, which found that biomass-specific rates of phagotrophy among pigmented flagellates (including autotrophic flagellates, dinoflagellates and prymnesiophytes) were half the rates, on average, compared with similarly sized non-pigmented cells (Stukel *et al.*, 2011). If this additional biomass is added to that of H-protists and regressed against grazing impacts as in Fig. 5, the relationship is still significant ($P < 0.0001$), but the slope is lower (1.54 μgC μgC^{-1} day^{-1}), translating to a lower mean consumer growth rate of 0.38 day^{-1} (Fig. 5). This is almost the same as the growth rate computed from the similar analysis of biomass-specific grazing including mixotrophs that was done for the equatorial Pacific upwelling region (Landry *et al.*, 2011). Both analyses are conservative, however, in neglecting additional carbon flows from H-Bact, detritus and intra-guild predation by protistan grazers, and, in the case of mixotrophs, the nutritional supplement from phototrophy. Thus, while mixotrophy was unmeasured and is unnecessary to explain the results of our study (i.e. taking a traditional perspective of distinct autotrophic and heterotrophic functions among protists reveals no obvious discrepancies in biomass and rate relationships), our results would also be consistent with a significant role of mixotrophic protists in the CRD. Like the top-down predatory impact of mesozooplankton, focused studies on mixotrophy may help us to explain signature features of the CRD such as the relatively modest regional variability in H-protist biomass, composition and productivity as well as the general maintenance of balanced production and grazing processes. Such studies are also needed to understand the resource acquisition strategies and trade-offs of nano-sized protists in the picophytoplankton-dominated, trace-element limited waters of the CRD.

SUPPLEMENTARY DATA

Supplementary data can be found online at http://plankt.oxfordjournals.org.

DATA ARCHIVING

Core data from this manuscript (H-protist abundance and biomass) are available through the Biological and Chemical Oceanography Data Management Office (http://www.bco-dmo.org/).

ACKNOWLEDGEMENTS

We thank the captain and crew of the R/V Melville and all cruise participants, particularly Darcy Taniguchi and Alexis Pasulka for collecting acid Lugol's samples and Takafumi Kataoka for collecting tintinnid samples.

FUNDING

The study was supported by US National Science Foundation grant OCE-0826626 to M.R.L.

REFERENCES

Agatha, S. (2004) A cladistic approach for the classification of oligotrichid ciliates (Ciliophora: Spirotricha). *Acta Protozool.*, **43**, 201–217.

Ahlgren, N. A., Noble, A., Patton, A. P., Roache-Johnson, K., Jackson, L., Robinson, D., McKay, C., Moore, L. R. *et al.* (2014) The unique trace metal and mixed layer conditions of the Costa Rica upwelling dome support a distinct and dense community of Synechococcus. *Limnol. Oceanogr.*, **59**, 2166–2184.

Azam, F., Fenchel, T., Field, J. G., Gray, J. G., Meyer-Reil, L. A. and Thingstad, F. (1983) The ecological role of water-column microbes in the sea. *Mar. Ecol. Prog. Ser.*, **10**, 257–263.

Barton, A. D., Finkel, Z. V., Ward, B. A., Johns, D. G. and Follows, M. J. (2013) On the roles of cell size and trophic strategy in North Atlantic diatom and dinoflagellate communities. *Limnol. Oceanogr.*, **58**, 254–266.

Beers, J. R. and Stewart, G. L. (1971) Micro-zooplankters in the plankton communities of the upper waters of the eastern tropical Pacific. *Deep Sea Res. I*, **18**, 861–883.

Binder, B. J., Chisholm, S. W., Olson, R. J., Frankel, S. L. and Worden, A. Z. (1996) Dynamics of picoplankton, ultraphytoplankton and bacteria in the central equatorial Pacific. *Deep Sea Res. II*, **43**, 907–931.

Calbet, A. (2008) The trophic roles of microzooplankton in marine systems. *ICES J. Mar. Sci.*, **65**, 325–331.

Calbet, A. and Landry, M. R. (2004) Phytoplankton growth, microzooplankton grazing, and carbon cycling in marine systems. *Limnol. Oceanogr.*, **49**, 51–57.

Calbet, A. and Saiz, E. (2005) The ciliate-copepod link in marine ecosystems. *Aquat. Microb. Ecol.*, **38**, 157–167.

Chavez, F. P., Buck, K. R., Service, S. K., Newton, J. and Barber, R. T. (1996) Phytoplankton variability in the central and eastern tropical Pacific. *Deep Sea Res. II*, **43**, 835–870.

Décima, M., Landry, M. R., Stukel, M. R., Lopez-Lopez, L. and Krause, J. W. (2016) Mesozooplankton biomass and grazing in the Costa Rica Dome: amplifying variability through the plankton food web. *J. Plankton Res.*, **38**, 317–330.

Dolan, J. (2012) Morphology and ecology in tintinnid ciliates of the marine plankton: correlates of lorica dimensions. *Acta Protozool.*, **49**, 235–244.

Esteban, G. F., Fenchel, T. and Finlay, B. J. (2010) Mixotrophy in ciliates. *Protist*, **161**, 621–641.

Fiedler, P. C. (2002) The annual cycle and biological effects of the Costa Rica Dome. *Deep Sea Res. I*, **49**, 321–338.

Franck, V. M., Smith, G. J., Bruland, K. W. and Brzezinski, M. A. (2005) Comparison of size-dependent carbon, nitrate, and silicic acid uptake rates in high- and low-iron waters. *Limnol. Oceanogr.*, **50**, 825–838.

Freibott, A., Linacre, L. and Landry, M. R. (2014) A slide preparation technique for light microscopy analysis of ciliates preserved in acid Lugol's fixative. *Limnol. Oceanogr. Meth.*, **12**, 54–62.

Garrison, D. L., Gowing, M. M., Hughes, M. P., Campbell, L., Caron, D. A., Dennett, M. R., Shalapyonok, A., Olson, R. J. *et al.* (2000) Microbial food web structure in the Arabian Sea: a US JGOFS study. *Deep Sea Res. II*, **47**, 1387–1422.

Green, J. C. (1991) Phagotrophy in prymnesiophyte flagellates. In Patterson, D. J. and Larsen, J. (eds.), *The Biology of Free-Living Heterotrophic Flagellates*. Vol. 45. Claredon Press, Oxford, pp. 401–414.

Gutiérrez-Rodríguez, A., Selph, K. E. and Landry, M. R. (2016) Phytoplankton growth and microzooplankton grazing dynamics across vertical environmental gradients determined by transplant *in situ* dilution experiments. *J. Plankton Res.*, **38**, 271–289.

Hwang, S. and Heath, R. T. (1997) The distribution of protozoa across a trophic gradient, factors controlling their abundance and importance in the plankton food web. *J Plankton Res.*, **19**, 491–518.

Kofoid, C. A. and Campbell, A. S. (1929) A conspectus of the marine and freshwater Ciliata belonging to the suborder Tintinnoinea, with descriptions of new species, principally from the Agassiz Expedition to the eastern tropical Pacific, 1904–1905. *Univ. Calif. Publ. Zool.*, **4**, 1–403.

Kofoid, C. A. and Campbell, A. S. (1939) Reports on the scientific results of the expedition to the Eastern Tropical Pacific, in charge of Alexander Agassiz, by the US Fish Commission steamer *Albatross*, from Oct. 1904 to Mar. 1905, Lieut.-Cdr. LM Garrett, USN, commanding. *Bull. Mus. Comp. Zool.*, **84**, 1–473.

Landry, M. R. and Calbet, A. (2004) Microzooplankton production in the oceans. *ICES J. Mar. Sci.*, **61**, 501–507.

Landry, M. R., Constantinou, J., Latasa, M., Brown, S. L., Bidigare, R. R. and Ondrusek, M. E. (2000) Biological response to iron fertilization in the eastern equatorial Pacific (IronEx II). III. Dynamics of phytoplankton growth and microzooplankton grazing. *Mar. Ecol. Prog Ser.*, **57**, 57–72.

Landry, M. R., Ohman, M. D., Goericke, R., Stukel, M. R. and Tsyrklevich, K. (2009) Lagrangian studies of phytoplankton growth and grazing relationships in a coastal upwelling ecosystem off Southern California. *Prog. Oceanogr.*, **83**, 208–216.

Landry, M. R., De Verneil, A., Goes, J. I. and Moffett, J. W. (2016a) Plankton dynamics and biogeochemical fluxes in the Costa Rica Dome: introduction to the CRD flux and zinc experiments. *J. Plankton Res.*, **38**, 167–182.

Landry, M. R., Selph, K. E., Décima, M., Gutiérrez-Rodríguez, A., Stukel, M. R., Taylor, A. G. and Pasulka, A. L. (2016b) Phytoplankton production and grazing balances in the Costa Rica Dome. *J. Plankton Res.*, **38**, 366–379.

Landry, M. R., Selph, K. E., Taylor, A. G., Décima, M., Balch, W. M. and Bidigare, R. R. (2011) Phytoplankton growth, grazing, and production balances in the HNLC equatorial Pacific. *Deep Sea Res. II*, **58**, 524–535.

Lessard, E. J. and Murrell, M. C. (1996) Distribution, abundance and size composition of heterotrophic dinoflagellates and ciliates in the Sargasso Sea near Bermuda. *Deep Sea Res. I*, **43**, 1045–1065.

Li, W. K. W., Rao, S., Harrison, W. G., Smith, J. C., Cullen, J. J., Irwin, B. and Platt, T. (1983) Autotrophic picoplankton in the tropical ocean. *Science*, **219**, 292–295.

Linacre, L., Landry, M. R., Cajal-Medrano, R., Lara-Lara, J. R., Hernández-Ayón, J. M., Mouriño-Pérez, R. R., García-Mendoza, E. and Bazán-Guzmán, C. (2012) Temporal dynamics of carbon flow through the microbial plankton community in a coastal upwelling system off northern Baja California, Mexico. *Mar. Ecol. Prog. Ser.*, **461**, 31–46.

Linacre, L., Landry, M. R., Lara-Lara, J. R., Hernández-Ayón, J. M. and Bazán-Guzmán, C. (2010) Picoplankton dynamics during contrasting seasonal oceanographic conditions at a coastal upwelling station of Northern Baja California, Mexico. *J. Plankton Res.*, **32**, 539–557.

Marshall, S. M. (1969) Protozoa: Order tintinnida, zooplankton sheets 117–127. In Fraser, J. H. and Hensen, V. Kr. (eds.), *Fiches d'identification du zooplancton.* Cons. Perm. Int. Explor. Mer, Charlottenlund.

Menden-Deuer, S. and Lessard, E. J. (2000) Carbon to volume relationships for dinoflagellates, diatoms, and other protist plankton. *Limnol. Oceanogr.*, **45**, 569–579.

Mertens, K. N., Yamaguchi, A., Yoshihito, T., Pospelova, V., Head, M. J., Radi, T., Pienkowski, A. J., de Vernal, A. *et al.* (2013) A new heterotrophic dinoflagellate from the north-eastern Pacific, Protoperidinium fukuyoi: cyst-theca relationship, phylogeny, distribution and ecology. *J. Eukaryot. Microbiol.*, **60**, 545–563.

Mitra, A., Flynn, J., Burkholder, J. M., Berge, T., Calbet, A., Raven, J. A., Granéli, E., Glibert, P. M. *et al.* (2014) The role of mixotrophic protists in the biological carbon pump. *Biogeosci.*, **11**, 995–1005.

Monger, B. C. and Landry, M. R. (1993) Flow cytometric analysis of marine bacteria with Hoechst 33342 *Appl. Environ. Microbiol.*, **59**, 905–911.

Naustvoll, L. J. (2000) Prey size spectra and food preferences in thecate heterotrophic dinoflagellates. *Phycologia*, **39**, 187–198.

Olseng, C. D., Naustvoll, L-J. and Eystein, P. (2002) Grazing by the heterotrophic dinoflagellate Protoperidinium steinii on a Ceratium bloom. *Mar. Ecol. Prog. Ser.*, **225**, 161–167.

Olson, M. B. and Daly, K. L. (2013) Micro-grazer biomass, composition and distribution across prey resource and dissolved oxygen gradients in the far eastern tropical north Pacific Ocean. *Deep Sea Res. I*, **75**, 28–38.

Pasulka, A. L., Landry, M. R., Taniguchi, D. A. A., Taylor, A. G. and Church, M. J. (2013) Temporal dynamics of phytoplankton and heterotrophic protists at station ALOHA. *Deep Sea Res. II*, **93**, 44–57.

Putt, M. and Stoecker, D. K. (1989) An experimentally determined carbon: volume ratio for marine "oligotrichous" ciliates from estuarine and coastal waters. *Limnol. Oceanogr.*, **34**, 1097–1103.

Saito, M. A., Rocap, G. and Moffett, J. W. (2005) Production of cobalt binding ligands in a *Synechococcus* feature at the Costa Rica upwelling dome. *Limnol. Oceanogr.*, **50**, 279–290.

Schmoker, C. and Hernández-León, S. (2013) Stratification effects on the plankton of the subtropical Canary Current. *Prog. Oceanogr.*, **119**, 24–31.

Selph, K. E., Landry, M. R., Taylor, A. G., Gutiérrez-Rodríguez, A., Stukel, M. R., Wokuluk, J. and Pasulka, A. L. (2016) Phytoplankton production and taxon-specific growth rates in the Costa Rica Dome. *J. Plankton Res.*, **38**, 199–215.

Sherr, E. B. and Sherr, B. F. (1993) Preservation and storage of samples for enumeration of heterotrophic protists. In Kemp, P. K. (ed.), *Handbook of Methods in Aquatic Microbial Ecology*. CRC Press, Boca Raton, Florida, pp. 207–212.

Sherr, E. B. and Sherr, B. F. (2002) Significance of predation by protists in aquatic microbial food webs. *Antonie van Leeuwenhoek*, **81**, 293–308.

Sherr, E. B. and Sherr, B. F. (2007) Heterotrophic dinoflagellates: a significant component of microzooplankton biomass and major grazers of diatoms in the sea. *Mar. Ecol. Prog. Ser.*, **352**, 187–197.

Sommer, U., Stibor, H., Katechakis, A., Sommer, F. and Hansen, T. (2002) Pelagic food web configurations at different levels of nutrient richness and their implications for the ratio fish production:primary production. *Hydrobiologia*, **484**, 11–20.

Stoecker, D. K. (1999) Mixotrophy among dinoflagellates. *J. Eukaryot. Microbiol.*, **46**, 396–401.

Stoecker, D. K. and Capuzzo, J. M. (1990) Predation on protozoa: its importance to zooplankton. *J. Plankton Res.*, **12**, 891–908.

Straile, D. (1997) Gross growth efficiencies of protozoan and metazoan zooplankton and their dependence on food concentration, predator-prey weight ratio, and taxonomic group. *Limnol. Oceanogr.*, **42**, 1375–1385.

Stukel, M. R., Landry, M. R. and Selph, K. E. (2011) Nanoplankton mixotrophy in the eastern equatorial Pacific. *Deep Sea Res. II*, **58**, 378–386.

Taylor, A. G., Landry, M. R., Freibott, A., Selph, K. E. and Gutiérrez-Rodríguez, A. (2016) Patterns of microbial community biomass, composition and HPLC diagnostic pigments in the Costa Rica upwelling dome. *J. Plankton Res.*, **38**, 183–198.

Taylor, A. G., Landry, M. R., Selph, K. E. and Yang, E. J. (2011) Biomass, size structure and depth distributions of the microbial community in the eastern equatorial Pacific. *Deep Sea Res. II*, **58**, 342–357.

Unrein, F., Gasol, J. M., Not, F., Forn, I. and Massana, R. (2014) Mixotrophic haptophytes are key bacterial grazers in oligotrophic coastal waters. *ISME J.*, **8**, 164–176.

Utermöhl, V. H. (1931) Neue Wege in der quantitativen Erfassung des Planktons. *Verh. Int. Verein. Theor. Angew. Limnol.*, **5**, 567–596.

Verity, P. G. and Langdon, C. (1984) Relationships between lorica volume, carbon, nitrogen, and ATP content of tintinnids in Narragansett Bay. *J. Plankton Res.*, **6**, 859–868.

Verity, P. G., Stoecker, D. K., Sieracki, M. E. and Nelson, J. R. (1996) Microzooplankton grazing of primary production at 140 W in the equatorial Pacific. *Deep Sea Res. II*, **43**, 1227–1255.

Vørs, N., Buck, K. R., Chavez, F. P., Eikrem, W., Hansen, L. E., Østergaard, J. B. and Thomsen, H. A. (1995) Nanoplankton of the equatorial Pacific with emphasis on the heterotrophic protists. *Deep Sea Res. II*, **42**, 585–602.

Wyrtki, K. (1964) Upwelling in the Costa Rica dome. *Fish. Bull.*, **63**, 355–372.

Yang, E. J., Choi, J. K. and Hyun, J. -H. (2004) Distribution and structure of heterotrophic protist communities in the northeast equatorial Pacific Ocean. *Mar. Biol.*, **146**, 1–15.

Yang, E. J., Choi, J. K. and Hyun, J-H. (2008) Seasonal variation in the community and size structure of nano- and microzooplankton in Gyeonggi Bay, Yellow Sea. *Estuar. Coast Shelf. S.*, **77**, 320–330.

Zhang, W., Feng, M., Yu, Y., Zhang, C., Sun, J. and Ziao, T. (2011) Species checklist of contemporary tintinnids (Ciliophora, Spirotrichea, Choreotrichia, Tintinnida) in the world. *Biodiv. Sci.*, **19**, 655–660.